(Received 13 March 2024, Accepted 27 April 2024, Scheduled 29 April 2024)

High Isolated Defected Ground Structure Based Elliptical Shape Dual Element MIMO Antenna for S-Band Applications

Praveen Kumar[1], Ajit K. Singh[2], Ranjeet Kumar[1], Rashmi Sinha[1], Santosh K. Mahto[1], Arvind Choubey[3], and A. J. A. Al-Gburi[4, *]

[1] *National Institute of Technology Jamshedpur, 831014, India*
[2] *Indian Institute of Information Technology Ranchi, 834010, India*
[3] *Department of Electronics & Communication Engineering, NIT Durgapur, West Bengal, India*
[4] *Center for Telecommunication Research & Innovation (CeTRI)*
Fakulti Teknologi dan Kejuruteraan Elektronik dan Komputer (FTKEK)
Universiti Teknikal Malaysia Melaka (UTeM)
Jalan Hang Tuah Jaya, Durian Tunggal, Melaka 76100, Malaysia

ABSTRACT: This research suggests a compact, wideband Multiple Input Multiple Output (MIMO) antenna designed for S-band applications, emphasizing high isolation between closely positioned antenna elements. Achieving this isolation is accomplished through the implementation of a Defected Ground Structure (DGS) technique. The DGS is realized by etching two elliptical patterns on an economical FR-4 substrate with inherent loss properties. Three rectangular slots and two L-shaped stubs are introduced to improve isolation and minimize the size of antenna increment by lowering surface wave propagation. To validate the proposed layout, a physical prototype was constructed for a direct comparison of its performance with the simulated parameters. The results demonstrated highly favorable outcomes, including Diversity Gain (DG) exceeding 9.97 dB, Envelope Correlation Coefficient (ECC) registering below 0.05, Mean Effective Gain (MEG) lower than -3 dB, Total Active Reflection Coefficient (TARC) below 0.4, and Channel Capacity Loss (CCL) less than 0.3. Furthermore, the current distribution and radiation pattern were found to be highly suitable for applications in the S-band and the lower part of the C-band, encompassing technologies like Bluetooth, WiFi, WiMAX, 4G, and 5G.

1. INTRODUCTION

MIMO antenna is indeed a critical technology in achieving high data rate transfers over communication channels in current and future generations of wireless communication systems. MIMO antenna is characterized by high data rate [1], spectral efficiency [2], substantial channel capacity [3], and robustness of the communication link [4]. To attain compact dimensions, it is normally necessary to have a relatively tiny spacing between consecutive elements of the antenna. A primary challenge in a MIMO antenna design revolves around striking the right balance between closely spaced antennas while ensuring adequate isolation between them. Due to the compactness of the terminals, MIMO systems suffer from significant mutual coupling, which can negatively impact the system's functionality by decreasing channel volume, bandwidth, and efficiency [5]. As a result, the mutual coupling between nearly placed antenna elements is the major factor that must be considered and maintained as low as possible without expanding antenna dimensions.

There are several techniques in literature to overcome the above problem, such as decoupling networks [6], parasitic element [7], split ring resonator (SRR) [8], microstrip open-loop resonator [8], electromagnetic band gap structure (EBG) [9, 10], and DGS [11–13]. However, due to its periodic nature, the EBG architecture is more complex in design and larger in size. The DGS technique is the most straightforward and least complicated design of the mutual coupling reduction strategies discussed above. This is achieved by creating a series of slits or slots on the ground, a technique employed to enhance the isolation between adjacent antennas [14–21]. A DGS operates similarly to a resonant LC circuit, functioning as a stopband filter. This stopband filter is employed to suppress surface waves between closely spaced antennas within the desired frequency range, effectively enhancing the isolation.

In this paper, we provide two closely spaced elliptical shape patch antennas. Three rectangular slots are introduced, and two simple L-shaped patterns are incised on the bottom to introduce a DGS which acts as a resonant slot and enhances the isolation. The distance between the antennas that are close together is significantly lowered by 10 mm ($0.071\lambda_0$). At 2.72 GHz, the maximum isolation -59.4 dB is achieved. The proposed MIMO antenna is compact, with dimensions of $0.344\lambda_0 \times 0.322\lambda_0$ ($48 \times 45\,\text{mm}^2$), and it operates across a frequency band spanning from 2.15 GHz to 5.65 GHz. This frequency range makes it well suited for applications in the S-band and C-band, including but not limited to Bluetooth, WiFi, WiMAX, 4G, and 5G technologies.

This prompted us to develop and test an elliptical microstrip 1×2 MIMO antenna for S- and C-band applications. This ar-

* Corresponding author: Ahmed Jamal Abdullah Al-Gburi (ahmedjamal@utem.edu.my, ahmedjamal@ieee.org).

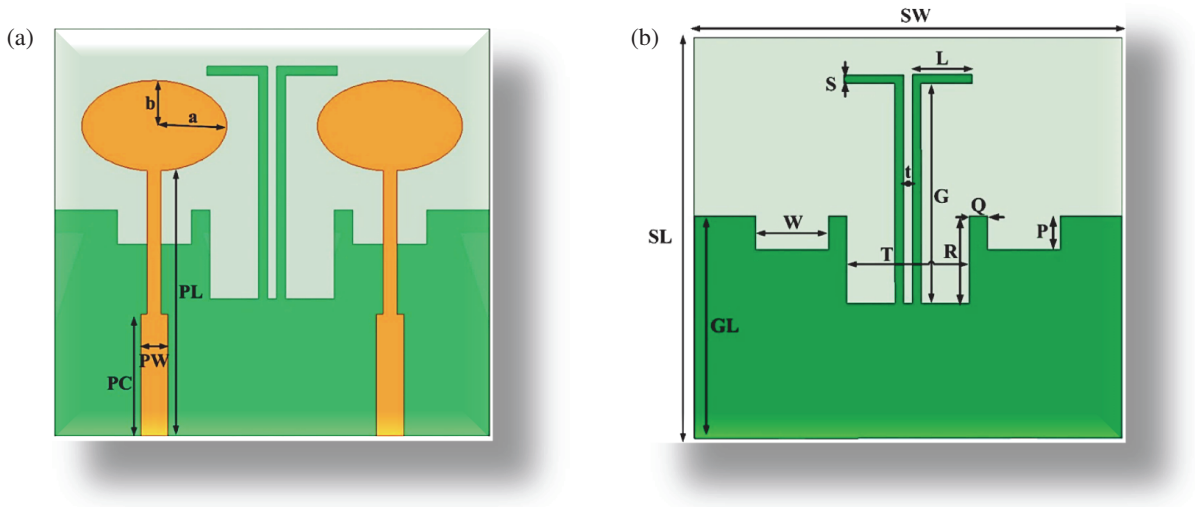

FIGURE 1. Rendered (a) upper and (b) lower perspectives of the envisaged MIMO antenna design.

ticle proposes a two-element MIMO antenna with an inverted L-shaped stub and three rectangular slots associated in the partial ground plane that takes up less space and good impedance bandwidth. The goal of using a MIMO antenna is to make use of its multipath capabilities, which enable higher data speeds, better channel capacity, interference mitigation, and improved signal dependability by preventing fading.

A detailed description of the DGS employed in the antenna is provided in Section 2. The performance parameters, both simulated and measured, are thoroughly analyzed and discussed in Sections 3 & 4, respectively. Finally, the document concludes with Section 5.

2. ANTENNA DESIGN

Within this section, we present the layout procedure for the MIMO antenna designed with DGS technique. The creation of this innovative MIMO antenna occurs through a two-stage process, as depicted in Figure 1. In the initial step, two elliptical motifs are etched onto the substrate, as demonstrated in Figure 1(a). These etchings serve as the radiating elements for the antenna. The second stage of the process is illustrated in Figure 1(b), in which three rectangular slots are etched, followed by two L-shaped stubs being printed on the ground plane. After researching different designs that are widely available and could improve the isolation between nearly placed antennas, L-shaped stubs are proposed. To enhance both isolation and structural stability in the proposed layout, an L-shaped stub isolator is positioned beneath the substrate. The final L-shaped stubs-based MIMO antenna is designed on an inexpensive FR-4 lossy substrate with a thickness of 1.6 mm, loss-tangent $(\delta) = 0.025$, and dielectric constant $(\epsilon_r) = 4.3$. The refined layout parameters for the MIMO antenna and L-shaped stub are as follows: $SW = 48$ mm, $SL = 45$ mm, $GL = 25$ mm, $W = 8.15$ mm, $P = 5.3$ mm, $S = 7$ mm, $T = 13.7$ mm, $R = 11.3$ mm, $Q = 2.1$ mm, $G = 24.65$ mm, $L = 6.7$ mm, $PW = 3$ mm, $PL = 31.1$ mm, $PC = 15.25$ mm, $b = 5$mm, and $a = 9$ mm.

Figures 2(a) and (b) illustrate bottom and top views of a constructed MIMO antenna. The MIMO antenna prototype undergoes measurement using a PNA Microwave Vector Network Analyzer, specifically the N5222A model. A representative experimental configuration is depicted in Figure 2(c).

3. MODELLING AND IN-DEPTH EVALUATION OF OPERATIONAL PERFORMANCE

In this section, we evaluate the overall performance of the designed MIMO antenna through an analysis that includes radiation pattern, S-parameters, surface current distribution, and diversity metrics such as ECC, MEG, DG, TARC, and CCL. We conduct these assessments using the High-Frequency Structure Simulator (HFSS), which is readily available commercial software for simulation purposes. Figure 3 presents a comprehensive S-parameter analysis of different developmental stages of the designed prototype. The variations in reflection and transmission coefficients resulting from the incorporation of a Defected Ground Structure (DGS) and the addition of stubs to the ground plane are examined and displayed in Figures 3(a) and 3(b), respectively.

In Figure 3(a), it is evident that without the presence of an L-shaped stub, the bandwidth is notably wide; however, the isolation between elements is relatively low. Remarkably, the band characteristics remain virtually unchanged throughout the evolution stages, as illustrated in Figure 3(a). Figure 3(b) provides insight into the effectiveness of introducing L-shaped stubs, which significantly enhances the isolation between elements. The systematic evolution of the proposed DGS with an L-shaped stub-based MIMO antenna consists of the following steps: (i) partial ground, (ii) incorporation of three rectangular slots on the partial ground, and (iii) integration of two L-shaped stubs, as depicted in Figures 3(a) and 3(b).

Figure 4 provides a side-by-side comparison of the computed and measured S-parameter characteristics of the planned MIMO antenna. Within the frequency span from 2.15 GHz to 5.65 GHz, the antenna successfully achieves the required

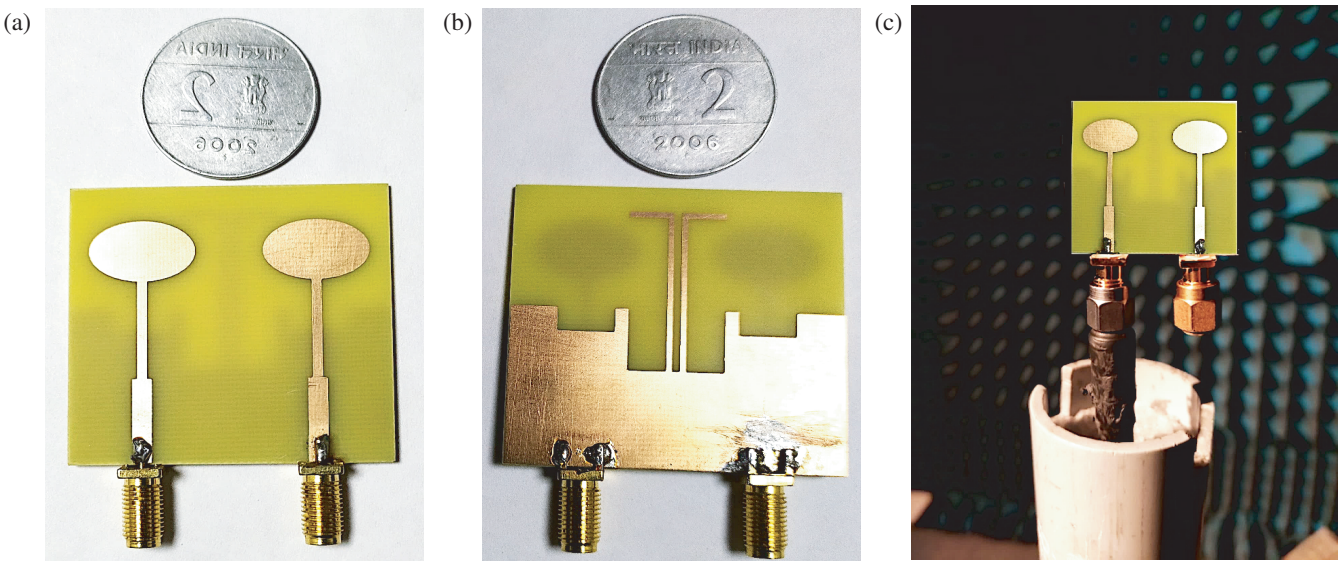

FIGURE 2. (a) Aerial perspective, (b) underbelly perspective, and (c) configuration for the practical arrangement of the envisaged MIMO antenna.

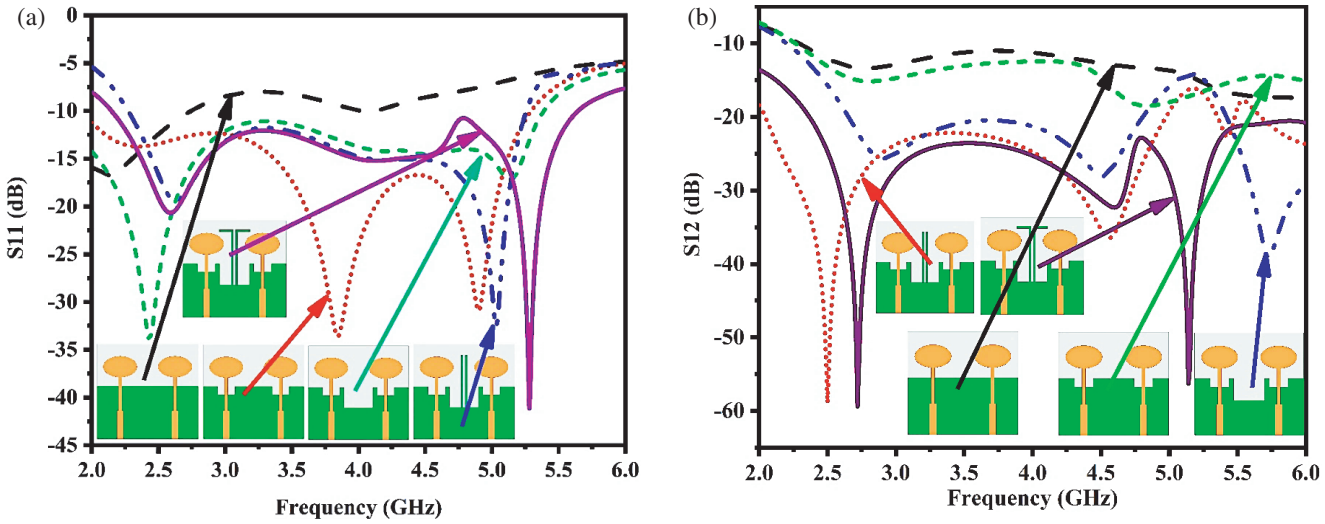

FIGURE 3. Evolutionary progression of the proposed antenna's S-parameters, showcasing (a) Reflection coefficient (S_{11}) and (b) Transmission coefficient (S_{21}).

3.5 GHz bandwidth. A noteworthy highlight is the antenna's maximum return loss (S_{11}) of -41 dB at 5.28 GHz. Moreover, the antenna exhibits exceptional isolation ($S_{12} \leq -20$ dB) between closely spaced antenna elements across the desired frequency range. The peak isolation value of -59.4 dB is particularly notable at 2.7 GHz. The introduction of L-shaped stubs to the design contributes significantly to enhancing the isolation, surpassing a 10 dB improvement.

Specifically, with L-shaped stubs, the peak values of S_{12} reach -59.4 dB at 2.7 GHz and -17.25 dB at 5.65 GHz, respectively. A careful examination of Figure 4 reveals an impressive alignment between the experimental and simulated results, highlighting the accuracy of the model.

Figure 5 illustrates the 2D radiation pattern, both predicted and measured, of the two-port MIMO antenna design at a frequency of 2.7 GHz. Notably, the radiation pattern exhibits distinct characteristics: at $\phi = 0°$, the pattern closely resembles that of a dipole antenna, while at $\phi = 90°$, it demonstrates omnidirectional radiation.

Figure 6 displays the surface current distribution of both antennas featuring a DGS. Examining the surface current provides clear insight into the impact of the DGS on the antenna system. When we apply an excitation to port-1 while port-2 is matched with a 50 Ω load, we observe surface currents moving from port 1 to port 2. Notably, a significant surface current is induced on port 1, which is effectively captured by the DGS structure.

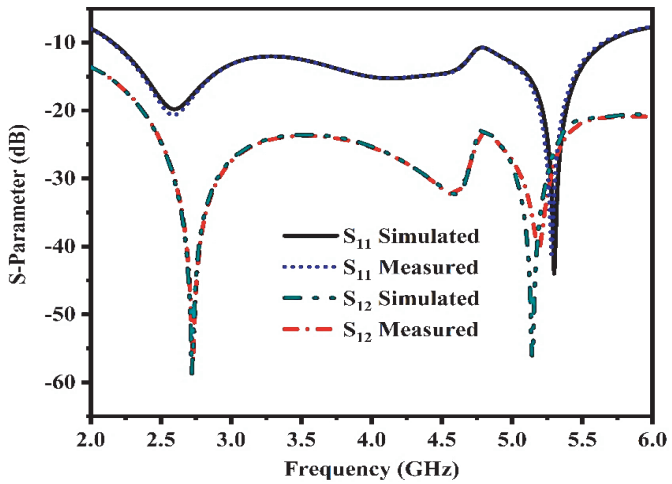

FIGURE 4. S-parameter of the modelled MIMO antenna.

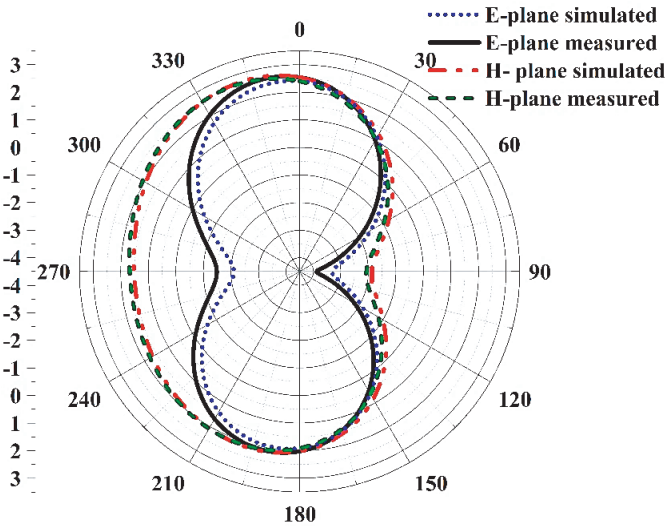

FIGURE 5. 2-D radiation pattern.

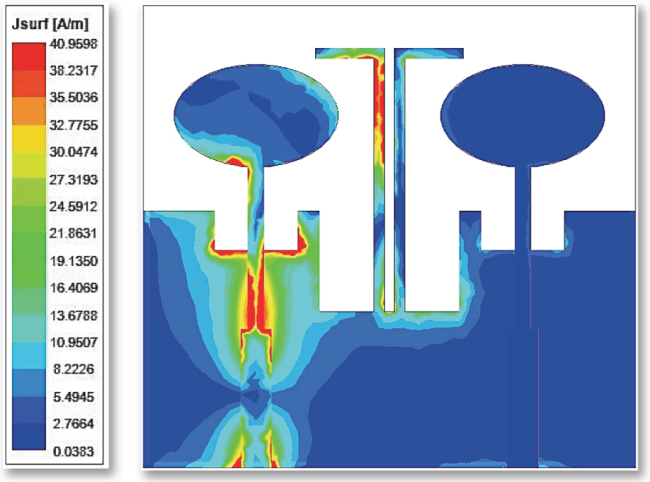

FIGURE 6. Magnitude of surface current density.

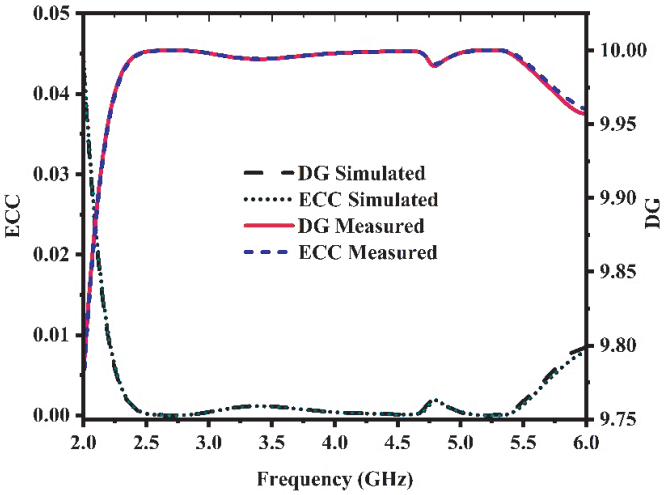

FIGURE 7. Simulated and Experimentally Obtained ECC and DG.

As a result, the high degree of isolation between Antenna 1 (Ant-1) and Antenna 2 (Ant-2) demonstrates the effectiveness of the proposed decoupling mechanism, particularly in the context of MIMO antenna applications.

4. DIVERSITY PERFORMANCE

When many antenna components are used, it is possible to quantify the degree to which their respective signal envelopes correlate using ECC. A signal's envelope refers to its magnitude independent of its phase. In addition to antenna coupling and mutual coupling between antennas, reflections and scattering from surrounding objects may contribute to an elevated ECC. To obtain a more accurate assessment, the ECC of MIMO the antenna should be estimated based on the radiated fields in [22]. Figure 7 illustrates that the ECC of the proposed MIMO antenna is less than 0.05. While the ideal ECC value is zero, in practical scenarios, an ECC below 0.5 is considered acceptable.

DG is another important parameter used to quantify the reduction in transmission power caused by the presence of DGS within a MIMO system [23].

As illustrated in Figure 7, the DG of the proposed MIMO antenna surpasses 9.97 dB. This value closely approaches the ideal benchmark of approximately 10 dB, signifying good diversity performance exhibited by the antenna.

TARC (Total Active Reflection Coefficient) is defined as the square root of the ratio of the total reflected power to the total incident power. It serves as a reliable indicator of MIMO antenna efficiency, encompassing valuable insights into mutual coupling effects [23, 24].

The actual value of TARC falls within the range of 0 to 1. When TARC equals zero, it signifies that all power is successfully transmitted, while a TARC value of one indicates that all power is either reflected or diverted to nearby ports. In the operational frequency band, both the predicted and measured TARCs of the planned MIMO system are found to be below 0.4, as presented in Figure 8(a).

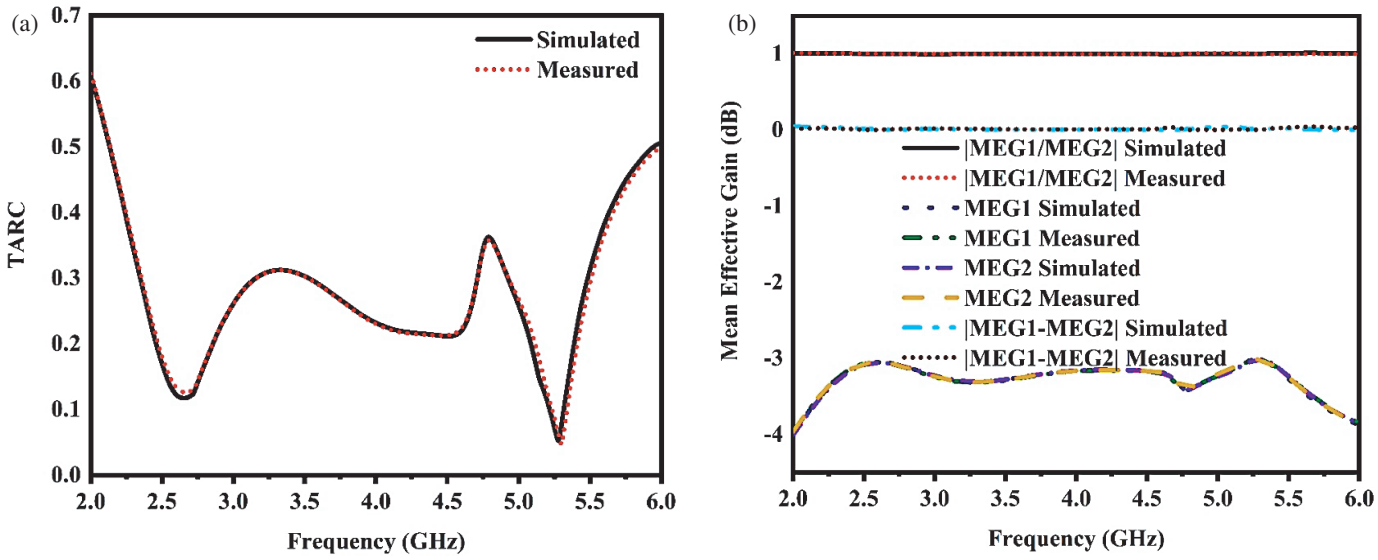

FIGURE 8. (a) TARC, (b) MEG.

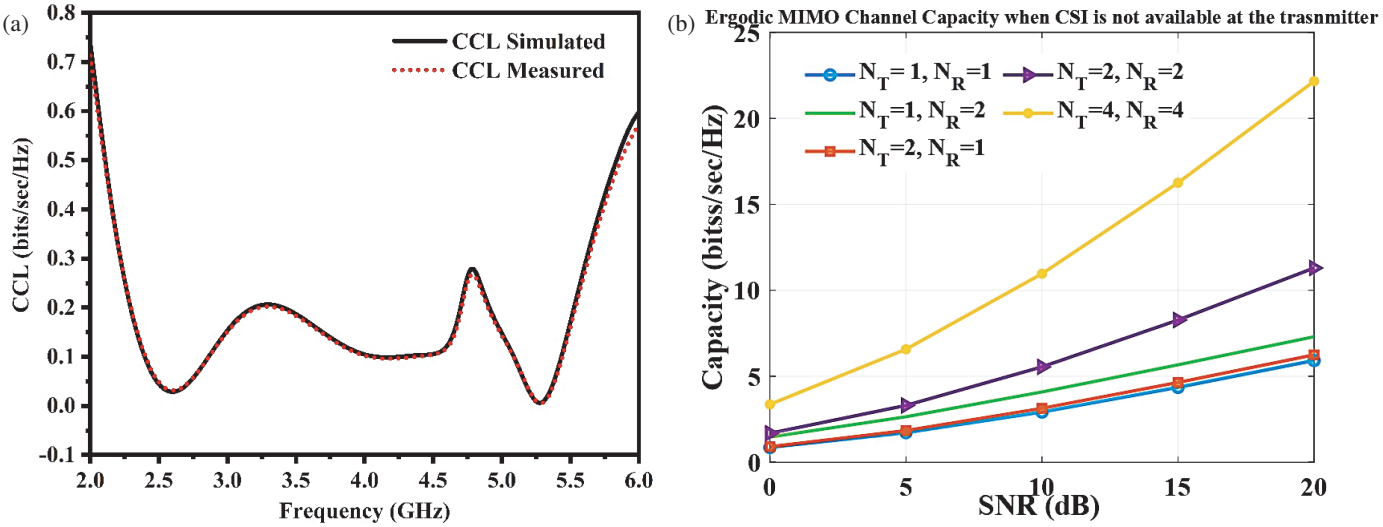

FIGURE 9. (a) CCL, (b) channel capacity.

The mean effective gain (MEG) serves as a pivotal metric for assessing the efficacy of MIMO diversity. It quantifies the power received by an isotropic antenna against the power acquired by the diversity antenna in a fading environment [25].

Figure 8(b) displays the Mean Effective Gain (MEG_i) for the desired frequency range, revealing values lower than -3 dB. This observation confirms the strong diversity performance of the proposed MIMO antenna.

Another essential metric for evaluating MIMO performance is the Coherent Channel Capacity (CCL), a measure of the maximum data delivery rate without substantial losses [25].

In order to excel in diversity performance, MIMO antennas are typically expected to maintain a CCL value below 0.4 bit/s/Hz. Figure 9(a) demonstrates that the proposed MIMO antenna achieves a CCL value lower than 0.3 bit/s/Hz, further underscoring its strong performance in diversity applications.

Channel capacity — The Ergodic Channel Capacity (CC), calculated under the assumption of no ECC between the transmitting antennas, stands out as a highly effective metric for MIMO system diversity characteristics. Equation (1) is applied to assess the channel matrix "H".

$$H = \sqrt{\rho_{scale,RX}} H_{iid} \sqrt{\rho_{scale,TX}} \tag{1}$$

In the context of the provided information, H_{iid} represents a 2×2 matrix comprising independently and identically distributed complex Gaussian random variables. The matrix $\rho_{scale,TX}$ is computed at the transmitter end, assuming null ECC and 100 percent efficiency. On the other hand, $\rho_{scale,RX}$ is derived by computing a 2×2 matrix using measured ECC and efficiency,

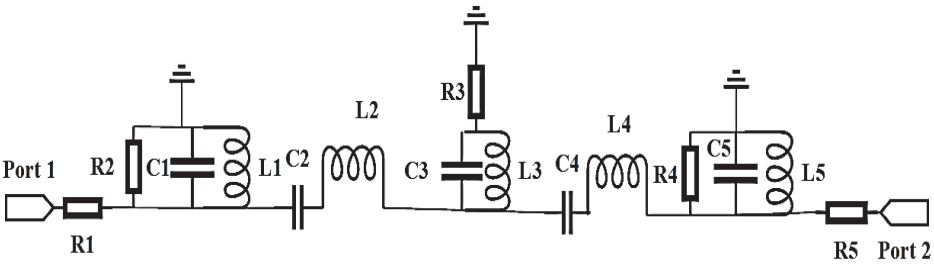

FIGURE 10. Schematic representation of the MIMO antenna system with its corresponding circuit diagram.

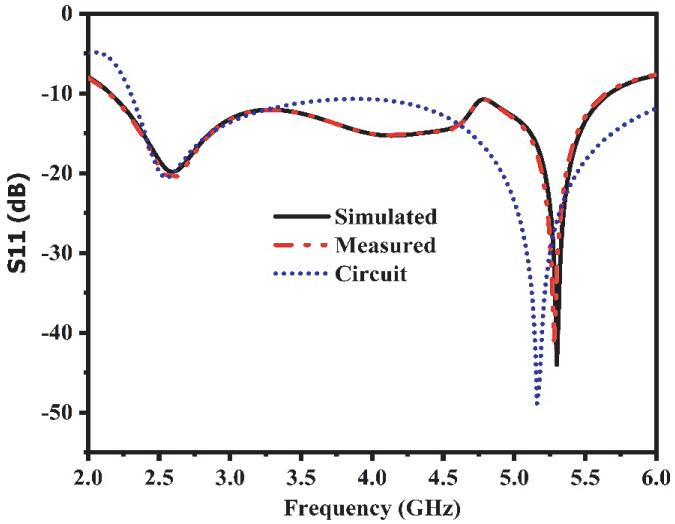

FIGURE 11. Reflection loss analysis for the proposed antenna, considering simulated, measured, and circuit model data.

as detailed in [21, 24] and Equation (2).

$$\rho_{scale,RX}\sqrt{n_{total}}\rho_{RX}\sqrt{n_{total}} \tag{2}$$

Equation (2) employs variables ρ_{RX} and n_{total}, corresponding to the efficiencies of receiving antennas, specifically ECC and total efficiency. To calculate the ergodic channel capacity, the estimation is carried out using Equation (3) [22]:

$$= E\left\{\log_2\left[\det\left(I + \frac{\text{SNR}}{n_T}HH^H\right)\right]\right\} \tag{3}$$

In Equation (3), the variables H^H, SNR, n_T, E, and I represent the Hermitian transpose, signal-to-noise ratio, number of antennas at the transmitter side, expectation with respect to various channel realizations, and a 4×4 identity matrix, respectively.

The theoretical channel capacities for 4×4 MIMO and 2×2 MIMO are 22.2 bps/Hz and 11.3 bps/Hz at an SNR of 20 dB, respectively. It is recommended that the channel capacity achieves at least 60% of the ideal value for optimal MIMO antenna performance [33]. In the simulated scenario, the channel capacity over the operating frequency bands is determined to be 10.62 bits/sec./Hz. The corresponding channel capacity versus frequency plot is illustrated in Figure 9(b).

The accurate electromagnetic simulation of antenna arrays often involves intricate configurations and resource-intensive computations, which is why equivalent circuit models are often preferred. Figure 10 displays the equivalent circuit model for the MIMO antenna design with a DGS. The equivalent circuit model of dual element MIMO antenna, where two patches are shown with resonant circuit resistors (R1, & R4), capacitors (C1, & C5), and inductors (L1, & L5), is shown in Figure 10. Within this circuit, the DGS is characterized by components such as L3, C3, and losses stemming from ohmic and dielectric effects, coupled with R3. The value of inductance relies on the metallic structure of the DGS, while capacitance is influenced by the separation distance between the metallic elements of the DGS. Antennas in close proximity exhibit mutual coupling, which is attributed to the inductance and capacitance of the DGS. Table 1 provides an overview of the optimized values for the elements within the equivalent circuit model. Figure 11 visually demonstrates a strong agreement between simulated return loss, measured loss, and the analysis conducted using the equivalent circuit model. It is evident that this model functions effectively across a frequency range spanning from 2.15 GHz to 5.65 GHz.

The designed MIMO antenna has been rigorously compared with recently published works, and the summarized findings are presented in Table 2. This MIMO antenna boasts a compact size of 48×45 mm^2, making it more space-efficient than most of its counterparts, with the exception of [18, 26, 29]. However, it is

TABLE 1. Optimal parameters for the circuit components.

Resistance (Ω)	Inductance (nH)	Capacitance (pF)
R_1= 02700	$L_1 = 203.87$	$C_1 = 03.32$
R_2= 47978	$L_2 = 444.86$	$C_2 = 01.16$
R_3= 00264	$L_3 = 418.54$	$C_3 = 09.88$
R_4= 13575	$L_4 = 250.00$	$C_4 = 21.16$
R_5= 17312	$L_5 = 32420.00$	$C_5 = 30.61$

TABLE 2. Comparative table.

Ref.	Dimension (mm)	Bandwidth (GHz)	Edge to edge gap	Max. Isolation (dB)	ECC
[8]	78 × 40	2.4–6.55 GHz (4.15 GHz)	10 mm	−35	0.1
[18]	32 × 32	3.1–10.6 GHz (7.5 GHz)	-	−30	0.02
[26]	50 × 30	2.5–14.5 GHz (12 GHz)	-	−50	0.04
[27]	75 × 150	3.3–5.0 GHz (1.7 GHz)	10 mm	−40	0.05
[28]	80 × 80	5.71–8.2 GHz (2.41 GHz)	23.29 mm	−25	0.05
[29]	50 × 22.5	5.23–6.42 GHz (1.19 GHz)	12.2	−40	0.001
[30]	66 × 66	1.8–2.6 GHz (0.8 GHz)	31.84 mm	≈ −40	0.01
[31]	95.9 × 38.2	2.43–2.50 GHz (0.07 GHz)	17 mm	−24.67 dB	0.0087
[32]	97 × 27.69	5.4–6.0 GHz (0.6 GHz)	13.75 mm	−43	0.0005
This work	48 × 45	4.27–10.1 GHz (5.83 GHz)	10 mm	−59	0.005

important to note that [18, 26] exhibit larger Equivalent Circuit Capacitance (ECC) values and weaker isolation compared to the antenna presented in this study. On the other hand, [29] features a larger separation between adjacent antenna edges and offers lesser isolation when being contrasted with the proposed design.

The proposed MIMO antenna stands out by achieving superior isolation compared to all other antennas listed in Table 2. While [18, 26] claim a larger bandwidth, they do so at the expense of poor isolation and a high ECC value. Additionally, [29, 32] exhibit low ECC, larger dimensions, and lower maximum isolation, making them less suitable for certain applications. In essence, the novel approach utilizing an L-shaped stub-based Defective Ground Structure (DGS) in this work presents a promising commercially viable solution to attain efficient isolation in MIMO antennas. Notably, it does not disrupt the primary radiation mode. This antenna design is particularly well suited for C-band applications, such as Bluetooth and Wi-Fi. Its exceptional isolation performance sets it apart from all the other antennas referenced in Table 2.

5. CONCLUSION

The MIMO antenna design featuring two L-shaped stubs is characterized by its compact, cost-effective, straightforward construction. It features a narrow gap of 10 mm (equivalent to $0.056\lambda 0$) between the antenna edges, effectively covering frequencies ranging from 2.15 GHz to 5.65 GHz. To ensure excellent isolation within the desired frequency range, the design incorporates two uncomplicated L-shaped stubs and three rectangular slots. At its peak, the antenna achieves an impressive isolation level of −59 dB at 2.7 GHz without compromising its bandwidth. These combined attributes make this antenna highly capable and suitable for deployment in the S band.

ACKNOWLEDGEMENT

The authors would like to thank Universiti Teknikal Malaysia Melaka (UTeM) and the Ministry of Higher Education (MOHE) of Malaysia for supporting this project.

REFERENCES

[1] Beigi, P., M. Rezvani, Y. Zehforoosh, J. Nourinia, and B. Heydarpanah, "A tiny ebg-based structure multiband MIMO antenna with high isolation for LTE/WLAN and C/X bands applications," *International Journal of RF and Microwave Computer-Aided Engineering*, Vol. 30, No. 3, e22104, 2020.

[2] Tse, D. and P. Viswanath, *Fundamentals of Wireless Communication*, Cambridge University Press, 2005.

[3] Chouhan, S., D. K. Panda, M. Gupta, and S. Singhal, "Meander line MIMO antenna for 5.8 GHz WLAN application," *International Journal of RF and Microwave Computer-Aided Engineering*, Vol. 28, No. 4, e21222, 2018.

[4] Hampton, J. R., *Introduction to MIMO Communications*, Cambridge University Press, 2013.

[5] Li, H., Y. Tan, B. K. Lau, Z. Ying, and S. He, "Characteristic mode based tradeoff analysis of antenna-chassis interactions for multiple antenna terminals," *IEEE Transactions on Antennas and Propagation*, Vol. 60, No. 2, 490–502, 2012.

[6] Banerjee, J., A. Karmakar, R. Ghatak, and D. R. Poddar, "Compact CPW-fed UWB MIMO antenna with a novel modified Minkowski fractal defected ground structure (DGS) for high isolation and triple band-notch characteristic," *Journal of Electromagnetic Waves and Applications*, Vol. 31, No. 15, 1550–1565, 2017.

[7] Jiang, W. and W. Che, "A novel UWB antenna with dual notched bands for WiMAX and WLAN applications," *IEEE Antennas and Wireless Propagation Letters*, Vol. 11, 293–296, 2012.

[8] Li, L., Z.-L. Zhou, J.-S. Hong, and B.-Z. Wang, "Compact dual-band-notched UWB planar monopole antenna with modified SRR," *Electronics Letters*, Vol. 47, No. 17, 950–951, 2011.

[9] Elabd, R. H. and A. J. A. Al-Gburi, "Super-compact 28/38 GHz 4-port MIMO antenna using metamaterial-inspired EBG structure with SAR analysis for 5G cellular devices," *Journal of Infrared, Millimeter, and Terahertz Waves*, Vol. 45, No. 1, 35–65, 2024.

[10] Fu, Y. and N. Yuan, "Elimination of scan blindness in phased array of microstrip patches using electromagnetic bandgap materials," *IEEE Antennas and Wireless Propagation Letters*, Vol. 3, 63–65, 2004.

[11] Lim, J.-S., C.-S. Kim, D. Ahn, Y.-C. Jeong, and S. Nam, "Design of low-pass filters using defected ground structure," *IEEE Transactions on Microwave Theory and Techniques*, Vol. 53, No. 8, 2539–2545, 2005.

[12] Hou, D.-B., S. Xiao, B.-Z. Wang, L. Jiang, J. Wang, and W. Hong, "Elimination of scan blindness with compact defected ground structures in microstrip phased array," *IET Microwaves, Antennas & Propagation*, Vol. 3, No. 2, 269–275, 2009.

[13] Vazquez, C., G. Hotopan, S. V. Hoeye, M. Fernandez, L. F. Herran, and F. Las-Heras, "Defected ground structure for coupling reduction between probe fed microstrip antenna elements," *PIERS Proceedings*, Cambridge, 2010.

[14] Wei, K., J. Li, L. Wang, Z. Xing, and R. Xu, "S-shaped periodic defected ground structures to reduce microstrip antenna array mutual coupling," *Electronics Letters*, Vol. 52, No. 15, 1288–1290, 2016.

[15] Elabd, R. H. and A. J. A. Al-Gburi, "SAR assessment of miniaturized wideband MIMO antenna structure for millimeter wave 5G smartphones," *Microelectronic Engineering*, Vol. 282, 112098, 2023.

[16] Jetti, C. R., T. Addepalli, S. R. Devireddy, G. K. Tanimki, A. J. A. Al-Gburi, Z. Zakaria, and P. Sunitha, "Design and analysis of modified U-shaped four element MIMO antenna for dual-band 5G millimeter wave applications," *Micromachines*, Vol. 14, No. 8, 1545, 2023.

[17] Ali, A., M. E. Munir, M. Marey, H. Mostafa, Z. Zakaria, A. J. A. Al-Gburi, and F. A. Bhatti, "A compact MIMO multiband antenna for 5G/WLAN/WIFI-6 devices," *Micromachines*, Vol. 14, No. 6, 1153, 2023.

[18] Ren, J., W. Hu, Y. Yin, and R. Fan, "Compact printed MIMO antenna for UWB applications," *IEEE Antennas and Wireless Propagation Letters*, Vol. 13, 1517–1520, 2014.

[19] Thakur, E., N. Jaglan, A. Gupta, and A. J. A. Al-Gburi, "Multi-band notched circular polarized MIMO antenna for ultra-wideband applications," *Progress In Electromagnetics Research M*, Vol. 125, 87–95, 2024.

[20] Saeidi, T., A. J. A. Al-Gburi, and S. Karamzadeh, "A miniaturized full-ground dual-band MIMO spiral button wearable antenna for 5G and sub-6 GHz communications," *Sensors*, Vol. 23, No. 4, 1997, 2023.

[21] Din, I. U., A. Kiyani, S. I. Naqvi, A. J. A. Al-Gburi, S. M. Abbas, and S. Ullah, "A low-cost wideband MIMO antenna for IoT applications," in *2022 IEEE International Symposium on Antennas and Propagation and USNC-URSI Radio Science Meeting (AP-S/URSI)*, 2064–2065, Denver, CO, USA, 2022.

[22] Kumar, P., R. Sinha, A. Choubey, and S. K. Mahto, "A novel metamaterial electromagnetic band gap (MM-EBG) isolator to reduce mutual coupling in low-profile MIMO antenna," *Journal of Electronic Materials*, Vol. 51, No. 2, 626–634, 2022.

[23] Ali, A., M. E. Munir, M. M. Nasralla, M. A. Esmail, A. J. A. Al-Gburi, and F. A. Bhatti, "Design process of a compact tri-band MIMO antenna with wideband characteristics for sub-6 GHz, Ku-band, and millimeter-wave applications," *Ain Shams Engineering Journal*, Vol. 15, No. 3, 102579, 2024.

[24] Kumar, P., A. K. Singh, R. Kumar, S. K. Mahto, P. Pal, R. Sinha, A. Choubey, and A. J. A. Al-Gburi, "Design and analysis of low profile stepped feedline with dual circular patch MIMO antenna and stub loaded partial ground plane for wireless applications," *Progress In Electromagnetics Research C*, Vol. 140, 135–144, 2024.

[25] Glazunov, A. A., A. F. Molisch, and F. Tufvesson, "Mean effective gain of antennas in a wireless channel," *IET Microwaves, Antennas & Propagation*, Vol. 3, No. 2, 214–227, 2009.

[26] Iqbal, A., O. A. Saraereh, A. W. Ahmad, and S. Bashir, "Mutual coupling reduction using F-shaped stubs in UWB-MIMO antenna," *IEEE Access*, Vol. 6, 2755–2759, 2017.

[27] Zhao, A. and Z. Ren, "Wideband MIMO antenna systems based on coupled-loop antenna for 5G N77/N78/N79 applications in mobile terminals," *IEEE Access*, Vol. 7, 93 761–93 771, 2019.

[28] Varshney, G., R. Singh, V. S. Pandey, and R. S. Yaduvanshi, "Circularly polarized two-port MIMO dielectric resonator antenna," *Progress In Electromagnetics Research M*, Vol. 91, 19–28, 2020.

[29] Khan, I., Q. Wu, I. Ullah, S. U. Rahman, H. Ullah, and K. Zhang, "Designed circularly polarized two-port microstrip MIMO antenna for WLAN applications," *Applied Sciences*, Vol. 12, No. 3, 1068, 2022.

[30] Adam, I., M. N. M. Yasin, N. Ramli, M. Jusoh, H. A. Rahim, T. B. A. Latef, T. F. T. M. N. Izam, and T. Sabapathy, "Mutual coupling reduction of a wideband circularly polarized microstrip MIMO antenna," *IEEE Access*, Vol. 7, 97 838–97 845, 2019.

[31] Sharma, K. and G. P. Pandey, "Two port compact MIMO antenna for ISM band applications," *Progress In Electromagnetics Research C*, Vol. 100, 173–185, 2020.

[32] Malviya, L., R. K. Panigrahi, and M. Kartikeyan, "Circularly polarized 2 × 2 MIMO antenna for WLAN applications," *Progress In Electromagnetics Research C*, Vol. 66, 97–107, 2016.

[33] Singh, A. K., S. K. Mahto, P. Kumar, and R. Sinha, "Analysis of path loss and channel capacity in quad element MIMO antenna for terahertz communication systems," *International Journal of Circuit Theory and Applications*, Vol. 51, No. 3, 1460–1475, 2023.